



Special Feature: CAE and Simulation

Research Report

Computational Prediction of Macroscopic Mechanical Behavior in Multi-constituent Steels

Noritoshi Iwata, Ikumu Watanabe, Daigo Setoyama and Takamichi Iwata

Report received on Nov. 11, 2014

■ABSTRACT■ In automobiles, the improvement of material performance in terms of strength, ductility, and formability contributes significantly to the enhancement of end-product performance as improved collision safety and weight reduction for fuel efficiency. The control of heterogeneities at various scales is one key approach in the research and development of structural materials. In this paper, our recent research about computational predictions of macroscopic mechanical behaviors in multi-constituent steels is reviewed, where a computational approach based on the finite element method is employed to model the heterogeneity at a micro scale and to relate the deformation state of the microstructure to the macroscopic mechanical behavior. Advanced constitutive models are developed to characterize the anisotropy of plastic mechanical behaviors dependent on the crystal structure in ferrite crystal grains and the lamellar direction in pearlite colonies. Also, the morphology effect of the ferrite-pearlite duplex microstructure on the macroscopic property is investigated by comparing the simulations and experiments.

■KEYWORDS■ Crystal Plasticity, Microstructures, Multiscale Modeling, Finite Element Method, Constitutive Model, Steel, Elastoplasticity, Yield-point Phenomenon

1. Introduction

Steels are widely used as structural materials for automobiles and buildings because of their excellent mechanical properties. In automobiles, the improvement of material performance in terms of strength, ductility, and formability contributes significantly to the enhancement of end-product performance as improved collision safety and weight reduction for fuel efficiency. It is well known that the mechanical properties depend on the microstructure of some distinctive constituents such as ferrite, pearlite, martensite, and bainite in steels. The control of the microstructure is integral to designing the mechanical properties and is recognized as a key approach in the research and development of structural materials. Therefore, much research^(1,2) has been conducted to understand the relationship between the microstructure and the macroscopic mechanical properties, which is actually a classical research topic in solid mechanics. Some approaches have also been widely used in industrial R&D as classical mixture rules, semi-analytical approaches^(3,4) based on Eshelby's inclusion theory,⁽⁵⁾ and representative volume element (RVE) approaches⁽⁶⁻⁸⁾ based on computational

discretization methods. These mainly have differences in the handling of interaction effects between microscopic components, and the modeling methodology has proceeded from non-interaction to full interaction in the arbitrary morphology.

At the Iron and Steel Institute of Japan, a project for the prediction and control of deformation characteristics⁽¹⁾ (which was conducted from 1989 until 1994) developed a database of material constants based on the Swift-type work hardening law, which is one of the simplest hardening equations in metal plasticity for single-constituent steels on the basis of a huge number of experiments to characterize the dependency of several major factors such as alloy elements and scale factors. In this project, the macroscopic material responses of a dual-constituent steel were predicted by incorporating the database with a classic mixture rule and Weng's secant method.⁽³⁾ After this pioneering project, the fundamental methods, computational software, and resources have progressed notably; however, the prediction of the macroscopic mechanical behavior of steels from microscopic information is still challenging. The main obstacle is the microstructure complexity of general carbon steels, e.g., the morphology of the

microstructure is disorganized, and the mechanical behaviors of the microscopic constituents are unknown. In recent years, promising advanced experimental techniques with three/four-dimensional visualization and nano/microscopic testing approaches have been developed to overcome such obstacles.⁽⁹⁻¹²⁾ The development of extended modeling approaches has been required to effectively utilize such observed information for the prediction of macroscopic mechanical behavior, which involves extracting primary factors from raw observation data and establishing theoretical modeling.

In this context, we have studied the multiscale modeling of carbon steels to capture the macroscopic mechanical behavior on the basis of alloy elements and forming processes, which involves the research and development of an advanced design approach coupling material design with process design. In this paper, we introduce a series of studies about finite element modeling and analyses of ferrite-pearlite duplex microstructures.^(7,8,13)

2. Single-crystal Plasticity Modeling of Competing Strengthening Effects

Single-crystal plasticity is an established framework used to describe the mechanical behavior of a crystalline material in microstructure simulations. In the application of single-crystal plasticity to ferritic crystals, two difficulties are well known: the computational instability caused by 48 slip systems and the modeling of the strengthening effects including the yield-point phenomenon. Therefore, we proposed a new single-crystal plasticity framework based on a representative characteristic length to model the competing strengthening mechanisms and implemented it into a nonlinear finite element software program based on an implicit integration scheme.⁽⁷⁾

2.1 Single-crystal Plasticity Based on Representative Characteristic Length

Single-crystal plasticity characterizes the anisotropic inelastic behavior dependent on the crystal structure. In a rate-independent framework, the yield function of the α -th slip system is given as follows:

$$\phi^{(\alpha)} := |\tau^{(\alpha)}| - q^{(\alpha)} \leq 0, \quad (1)$$

where $\tau^{(\alpha)}$ is the resolved shear stress of the

α -th slip system, and $q^{(\alpha)}$ is the critical resolved shear stress (CRSS). The resolved shear stress is crystallographically defined with the so-called Schmid law, whereas the definition of the CRSS remains flexible. Here, we define the CRSS of the α -th slip system with the representative characteristic length $l^{(\alpha)}$ as follows:

$$q^{(\alpha)} := \tau_0^{(\alpha)} + \frac{\mu b}{l^{(\alpha)}}, \quad (2)$$

where $\tau_0^{(\alpha)}$ is the reference resolved shear stress of the α -th slip system, μ is the elastic shear constant, and b is the magnitude of the Burgers vector. Furthermore, the representative characteristic length $l^{(\alpha)}$ is defined to express a competitive relationship between the strengthening effects as

$$\begin{cases} l_\rho^{(\alpha)} & \text{if } l_\rho^{(\alpha)} \leq l_c^{(\alpha)} \\ l_c^{(\alpha)} & \text{if } l_\rho^{(\alpha)} > l_c^{(\alpha)} \end{cases} \quad \forall \alpha \in \{1, \dots, n_{\text{slip}}\}, \quad (3)$$

where $l_\rho^{(\alpha)}$ is the characteristic length of the dislocation density of the α -th slip system, and $l_c^{(\alpha)}$ is an internal characteristic length dependent on the strengthening factors except for the dislocation accumulation or plastic deformation history. The characteristic length $l_\rho^{(\alpha)}$ is defined as

$$l_\rho^{(\alpha)} = \frac{1}{a} \left(\sum_{\beta=1}^{n_{\text{slip}}} \Omega_{\alpha\beta} \rho^{(\beta)} \right)^{-1/2} \quad \forall \alpha \in \{1, \dots, n_{\text{slip}}\}, \quad (4)$$

where a is a weighting coefficient, $\Omega_{\alpha\beta}$ is an interaction matrix for the dislocation density of each slip system, and $\rho^{(\alpha)}$ is the dislocation density of the α -th slip system. If $l_\rho^{(\alpha)} \leq l_c^{(\alpha)}$, the CRSS of the α -th slip system Eq. (2) has a similar format as the Bailey-Hirsh⁽¹⁴⁾ relationship

$$q^{(\alpha)} = \tau_0 + a \mu^{(\alpha)} b \sqrt{\sum_{\beta=1}^{n_{\text{slip}}} \Omega_{\alpha\beta} \rho^{(\beta)}}. \quad (5)$$

In this study, the following equations are used to bridge between the dislocation densities and accumulated slips for all slip systems:

$$\rho^{(\alpha)} := \rho_{\text{sat}} \left(1 - \exp \left[-\frac{1}{\rho_{\text{sat}}} \frac{\xi^{(\alpha)}}{b \bar{x}^{(a)}} \right] \right) \quad \forall \alpha \in \{1, \dots, n_{\text{slip}}\}, \quad (6)$$

where ρ_{sat} is the maximum value of the dislocation density of a slip system, and $\bar{x}^{(a)}$ is a variable of the length dimension that exhibits the movability of the

dislocation and is assumed to be $\bar{\kappa}^{(a)} = c l^{(a)}$ with a material constant c .

2.2 Crystal Plasticity Finite Element Analysis to Characterize Yield-point Phenomenon

Using the above constitutive model, finite element analysis of periodic polycrystalline aggregate was performed to illustrate the yield-point elongation and the hardening behavior governed by the accumulation of dislocations, where the strengthening effect of the interstitial solid solution was considered within the internal characteristic length. The numerical results are shown in **Figs. 1** and **2**, where the macroscopic dislocation density is defined as the volume average of the total dislocation density in the RVE,

$$\tilde{\rho} := \frac{1}{|\mathcal{V}|} \int_{\mathcal{V}} \bar{\rho} dy, \quad (7)$$

where $|\mathcal{V}|$ is the volume of the RVE. Also, the evolution

of the macroscopic dislocation density was redrawn in **Fig. 3** to show that the Bailey-Hirsh relationship was reproduced in macroscopic response after yield-point elongation.

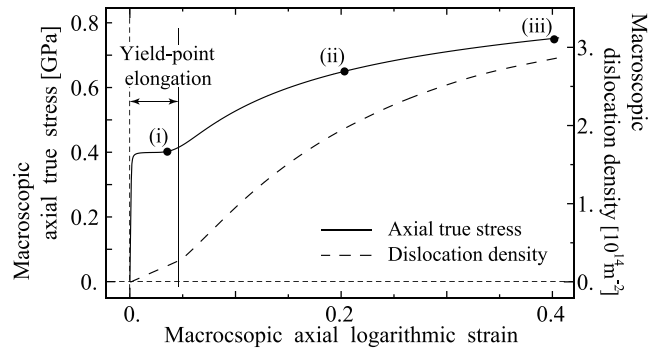


Fig. 1 Macroscopic axial stress-strain curve for polycrystalline aggregate with evolution of macroscopic dislocation density.

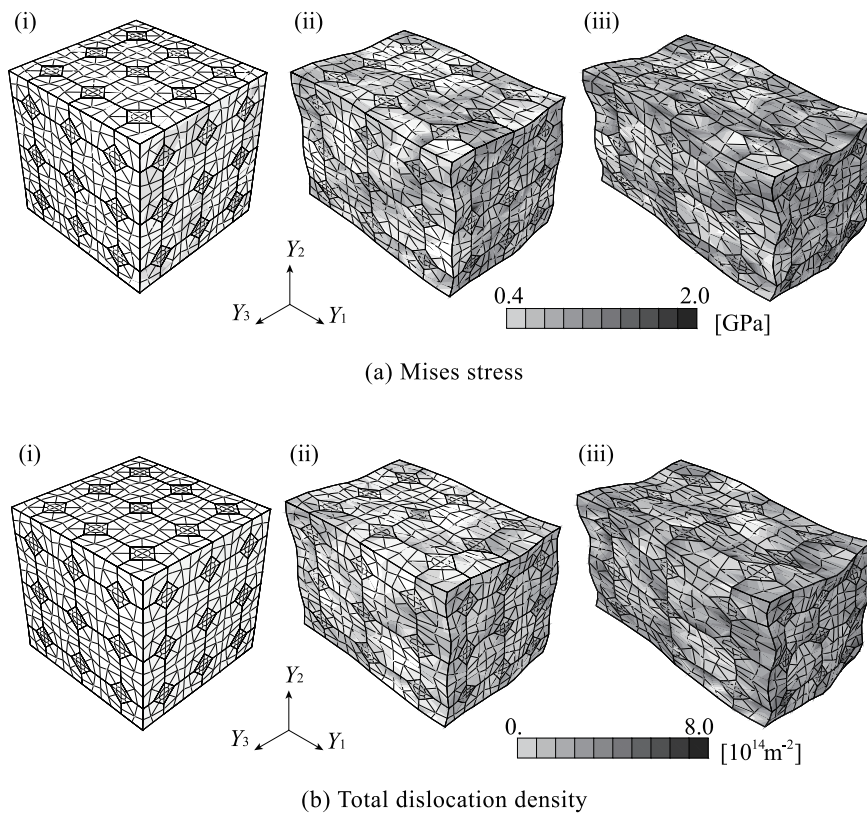


Fig. 2 Deformation state and distributions of Mises stress and total dislocation density in polycrystalline RVE model at three points on macroscopic stress-strain curve of Fig. 1: (a) distribution of Mises stress and (b) distribution of total dislocation density.

2.3 Modeling of Grain-size Strengthening Effect

The proposed constitutive model is also available to describe the grain size dependency of the initial yield stress. By preparing a finite element model with fine mesh inside a grain, the internal characteristic length was defined as the distance from the closest grain boundary. The macroscopic stress-strain curves for some cases with different grain sizes in the uniaxial tensile test are displayed in Fig. 4. Based on the results, the relationship between the grain size and the macroscopic 0.2% strain offset yield strength was depicted in Fig. 5. This figure presents the strengthening effect on the grain size, where the so-called Hall-Petch relationship^(15,16) was simulated in the range of practical polycrystalline metals.

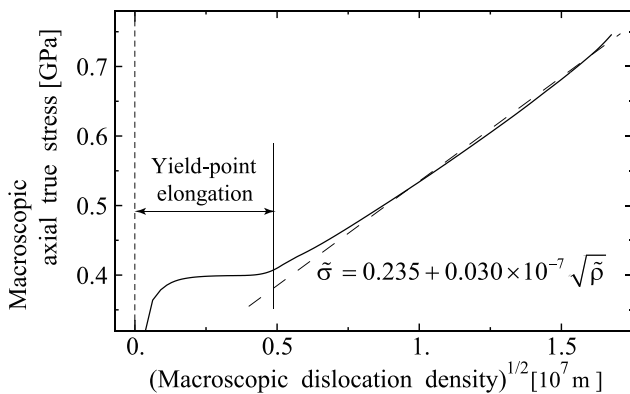


Fig. 3 Macroscopic relation between macroscopic axial stress and square root of macroscopic dislocation density for the polycrystalline aggregate.

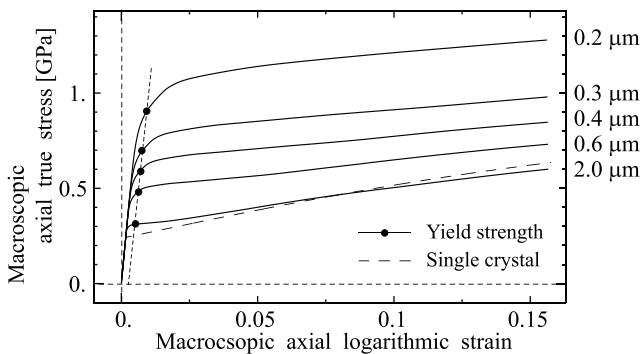


Fig. 4 Macroscopic axial stress-strain curves of examination for grain size dependency.

3. Constitutive Modeling of Pearlite Colony

Pearlite microstructure is composed of pearlite colonies characterized by the lamellar structure of the ferrite and cementite phases. An anisotropic elastic-plastic constitutive model for the pearlite colony was formulated within the multiscale modeling.⁽⁸⁾

3.1 Numerical Material Testing of Pearlite Colony

At first, the anisotropic mechanical behavior of the pearlite colony was examined with finite element analysis for a periodic microstructure. The finite element model of the periodic lamellar structure was constructed based on our experimental and theoretical knowledge. Here, a first principle calculation was performed to obtain elastic constants of cementite because it is difficult to estimate in experimental material tests due to the metastability of cementite.⁽⁸⁾ With the finite element model of the pearlite colony, numerical material testing was performed, i.e., the macroscopic material response was computationally examined for various macroscopic strain modes. The result shows that the interlamellar plastic deformation mode is dominant because it is independent from the constraint of the cementite phase. Also, the stress values of the cementite phase are unrealistically high in these numerical results except for the interlamellar shear deformation mode. It is quite likely that such a high stress state induces some dissipation mechanics, for example, the plastic behavior of the cementite phase or debonding at the boundary between the ferrite and cementite phases.

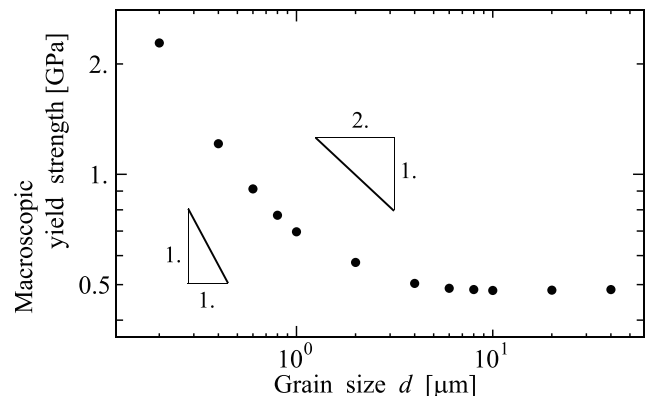


Fig. 5 Grain size effect on yield strength.

3.2 Formulation of Constitutive Equations

Based on the results of numerical material testing, we defined the plastic constitutive behavior of the pearlite colony as a two-stage yielding behavior: interlamellar shear yielding and the yielding of the overall microstructure. The two behaviors are written as two yield functions,

$$\begin{aligned} \psi^{(1)} &:= |\mathbf{s} \cdot (\boldsymbol{\tau} \mathbf{m})| - (\tau_Y^{(1)} + h_{11} \zeta^{(1)} + h_{12} \zeta^{(2)}) \leq 0 \\ \psi^{(2)} &:= \sqrt{\frac{3}{2} \text{dev}[\boldsymbol{\tau}] : \text{dev}[\boldsymbol{\tau}]} - (\tau_Y^{(2)} + h_{21} \zeta^{(1)} + h_{22} \zeta^{(2)}) \leq 0, \end{aligned} \quad (8)$$

where $\tau_Y^{(\alpha)}$ is the initial yield stress for the α -th yield function ($\alpha = 1$ or 2), $h_{\alpha\beta}$ ($\alpha, \beta = 1$ or 2) is the hardening coefficient containing cross-hardening, and $\zeta^{(\alpha)}$ ($\alpha = 1$ or 2) is an internal variable for the work hardening. The first yield function $\psi^{(1)}$ represents the slip behavior on the lamella described by its normal vector \mathbf{m} , where the slip direction \mathbf{s} is calculated from the stress state. It is noted that the second yield function $\psi^{(2)}$ described with standard isotropic plasticity is indispensable for reproducing the experimental stress-strain curves in simulations. The evolution equations of the internal variables and the computational procedures were formulated within the framework of standard multi-surface plasticity, which is the same as single-crystal plasticity.⁽⁷⁾ The evolution equations are given as follows:

$$\begin{aligned} \mathbf{L}^p &= \sum_{\alpha=1}^2 \gamma^{(\alpha)} \frac{\partial \psi^{(\alpha)}}{\partial \hat{\mathbf{T}}} = \sum_{\alpha=1}^2 \gamma^{(\alpha)} \mathbf{N}^{(\alpha)}, \\ \dot{\zeta}^{(\alpha)} &= \gamma^{(\alpha)}, \quad \alpha \in \{1, 2\}, \end{aligned} \quad (9)$$

where $\mathbf{N}^{(\alpha)}$ is a plastic flow tensor of the α -th yield function.

The macroscopic stress-strain curves of the pearlite colony for some strain modes were reproduced with the proposed constitutive model as shown in Fig. 6. Two types of simple shear deformation modes (H_{13} and H_{31}) initially exhibit yielding behavior, and isotropic yielding causes other plastic deformation modes like H_{11} . The material response of H_{31} increases the stiffness and becomes a coupling plastic behavior with the isotropic plasticity describing the yielding of the overall microstructure.

3.3 Finite Element Analyses of Ferrite-pearlite Duplex Steels

Using the abovementioned constitutive models for the ferrite crystal and pearlite colony, finite element analyses were performed to predict the mechanical behavior of ferrite-pearlite duplex steels. A basic finite element model is prepared as shown in Fig. 7, which satisfies the geometrical periodicity condition and is composed of 54 blocks. Each block is recognized as either ferrite or pearlite and is assumed to be discretely distributed like the microstructure shown in Fig. 8. The orientations of each ferrite crystal grain and pearlite colony are provided in a random fashion. As

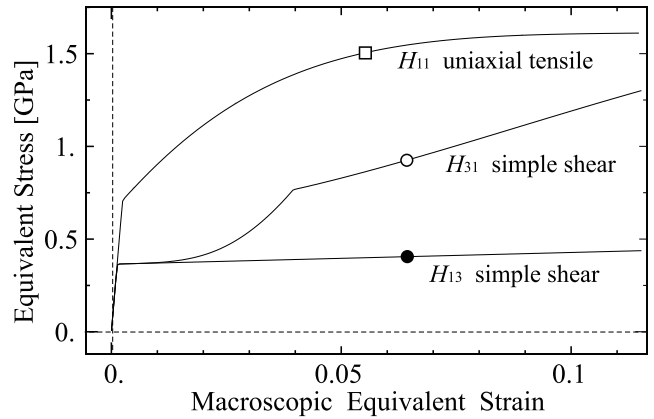


Fig. 6 Anisotropic equivalent stress-strain curves of constitutive model of pearlite colony.

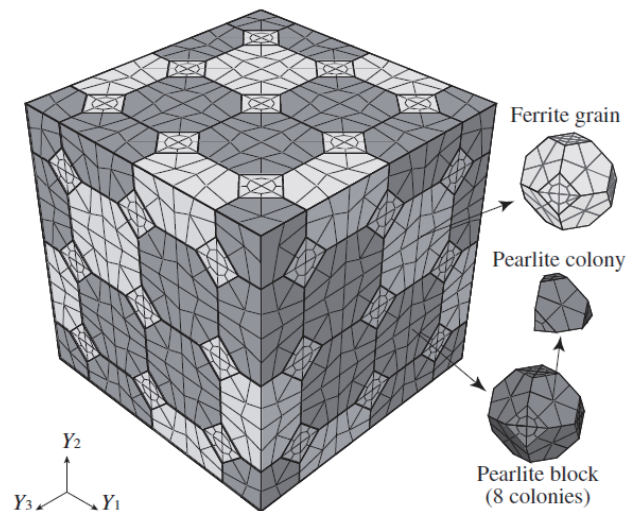


Fig. 7 Finite element model of microstructure of ferrite-pearlite steel.

presented in **Fig. 9**, the numerical results surely had good agreement with the corresponding experiments in the macroscopic material response. Here, we compared the microscopic deformation states between the computational results and the experiments for the validation of the simulations by utilizing a digital image correlation method⁽¹⁷⁾ to visualize the strain distribution in the experiments.

The distributions of equivalent stress and maximum principal strain are depicted in **Fig. 10** for a macroscopic axial strain of 15%. The stress states in the ferrite grains significantly differ from those in the pearlite blocks, and the ferrite grains had a larger plastic deformation than the pearlite blocks with the strength difference. In the experiment, a qualitatively similar strain distribution was obtained, as illustrated

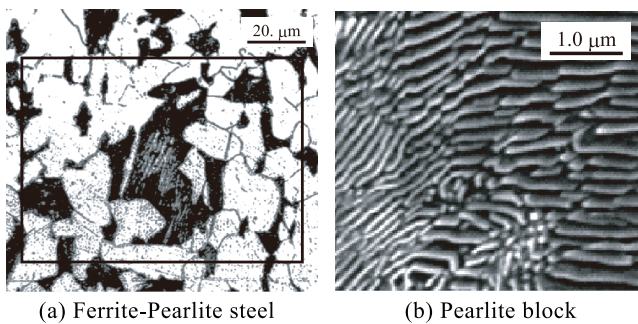


Fig. 8 Hierarchical microstructure of ferrite-pearlite steel. (a) Ferrite-pearlite steel and (b) Pearlite block.

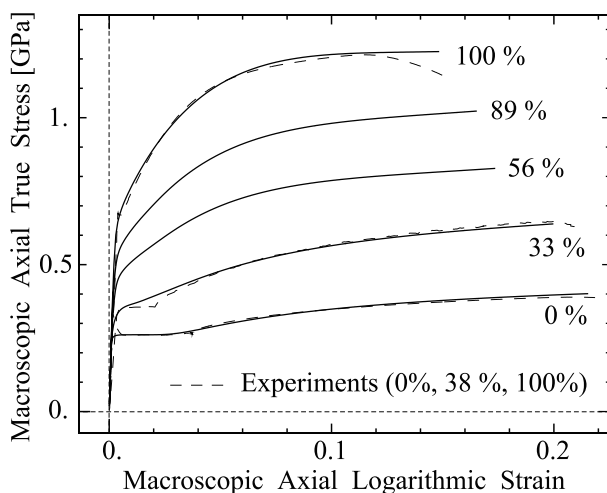


Fig. 9 Macroscopic axial stress-strain curves of ferrite-pearlite steel.

in **Fig. 11(b)**, which was calculated from the deformation state of **Fig. 11(a)**.

4. Morphology Effect of Ferrite-pearlite Duplex Microstructure

The morphology effect of the ferrite-pearlite duplex microstructure on the macroscopic mechanical behavior is investigated by a comparison between the numerical and experimental material tests.⁽¹³⁾

4.1 Simulations and Experiments

In this study, we focused on the strengthening effect of the microscopic morphologic heterogeneity in ferrite-pearlite duplex steels. To reduce computational

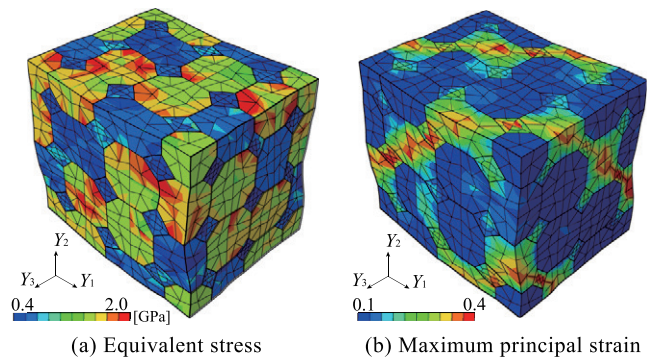


Fig. 10 Microscopic stress and strain distributions for ferrite-pearlite steel (pearlite volume fraction 33% at a point of macroscopic axial strain 15%). (a) Equivalent stress and (b) Maximum principal strain.

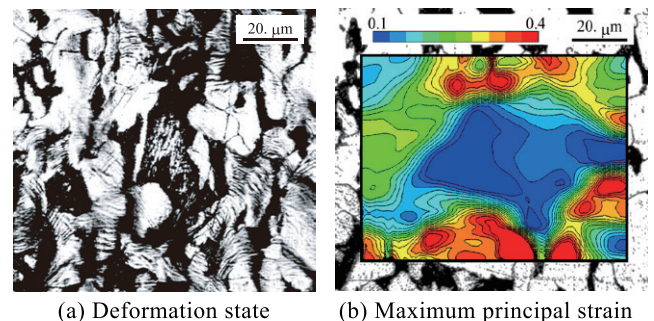


Fig. 11 Microscopic deformation state and strain distribution from experimental data (ferrite-pearlite steel of pearlite volume fraction 38% at a point of axial strain 15%). (a) Deformation state and (b) Maximum principal strain.

efforts and to simplify the modeling, an isotropic constitutive model was employed to describe the mechanical behaviors of the two constituents. The stress-strain relationships of the two constituents are shown in Fig. 12. Actually, the difference in strengths between these two constituents is a major heterogeneity, so such a simple modeling method works well for the prediction of the macroscopic material response. However, it is noted that the heterogeneity in each constituent becomes dominant in the cases where their volume fractions lean to one side.

Here, three kinds of finite element models were prepared for ferrite-pearlite duplex steels, as illustrated in Fig. 13, where the series of model A and model B possess the core-shell structure composed

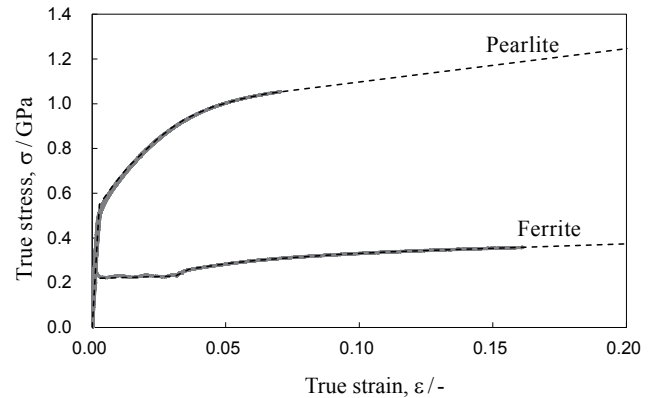


Fig. 12 Stress-strain curves of ferrite single-phase steel and full-pearlite steel. The solid and the dashed lines indicate experimental and numerical results, respectively.

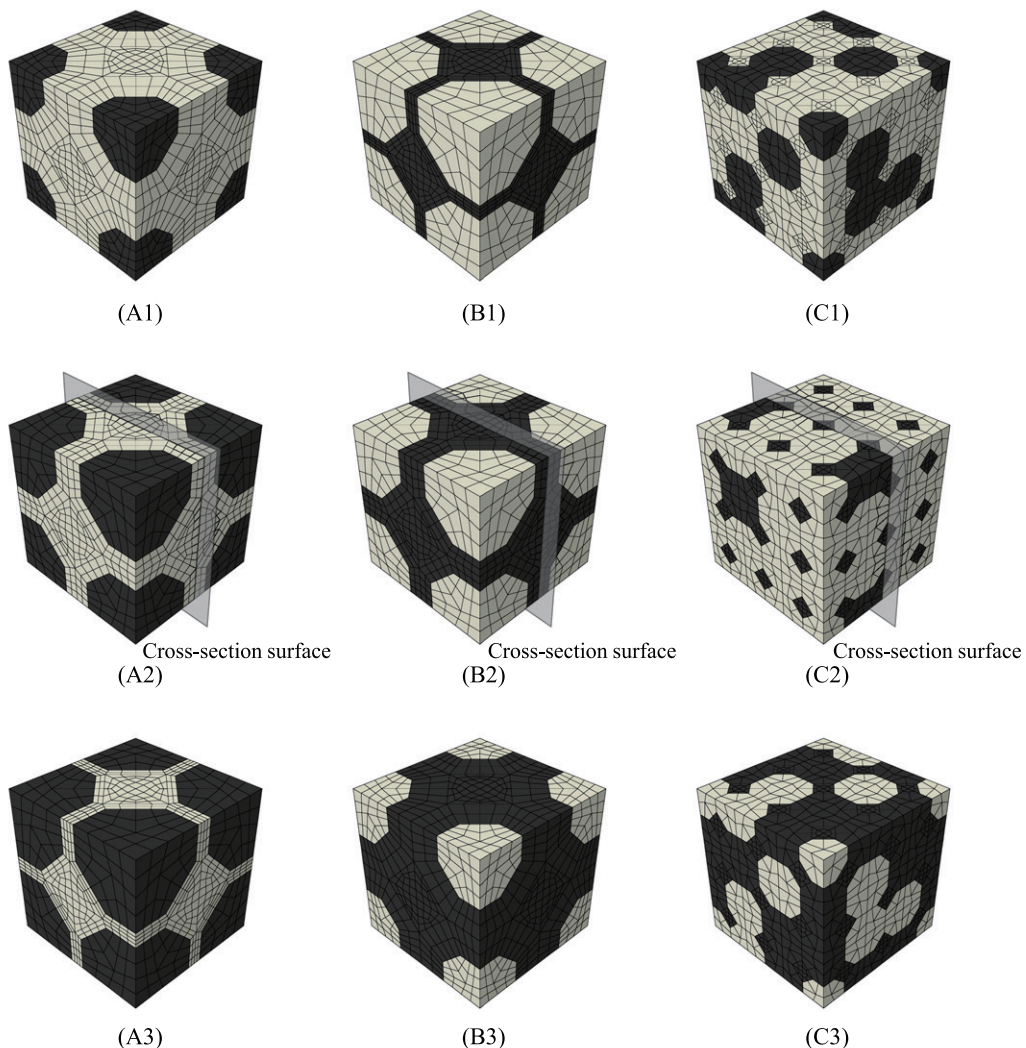


Fig. 13 Finite element models of microstructure of ferrite-pearlite duplex steels with different pearlite volume fraction. Model A: (A1) 21.6%, (A2) 51.2%, (A3) 72.9% Model B: (B1) 27.1%, (B2) 48.8%, (B3) 78.4% Model C: (C1) 22.2%, (C2) 55.6%, (C3) 77.8%

of connecting and distributed components, i.e., the microstructure containing the matrix and inclusion. Ferrite is the matrix in model A, whereas pearlite is the matrix in model B. In model C, each phase is randomly distributed in the same manner as shown in Fig. 8. Case studies for some volume fractions of ferrite or pearlite for these three models were performed to characterize the dependency of the microscopic morphology and volume fraction on the macroscopic mechanical behavior.

To obtain the corresponding experimental results, specimens changing the volume fraction of pearlite were fabricated, where it was assumed that we could control the volume fraction of pearlite by the carbon content because almost all of the carbon was considered to be used for the pearlite in the thermal fabrication processes. Also, the ferrite grain size and lamellar spacing were carefully adjusted to around 10 μm and 0.15 μm , respectively, in order to remove the major strengthening factors except for the volume fraction by controlling the heat treatment conditions.

4.2 Results and Discussions

The stress-strain curves for three pearlite volume fractions are shown in Fig. 14. The relationships between the stress value at 10% axial strain and the pearlite volume fraction are drawn in Fig. 15, in which the upper and lower bounds based on the same concept with the classical mixture rule are effective. The responses of model A and model B follow the upper and lower bounds, respectively, which is explainable based on the topology of the strong component. That of model C shifts from the lower bound to the upper bound with an increase in the volume fraction of pearlite because the topology of the strong component changes gradually, which is certainly the morphology effect on the macroscopic mechanical behavior. However, the tendency of the corresponding experiments shifts inversely from the upper bound to the lower bound with an increase in the volume fraction of pearlite. The cause of this result is the incompleteness of both our simulation models and the experimental samples; e.g., our current model cannot follow the stress dropping at the yield point shown in Fig. 14, and the yield-point phenomenon means that interstitial carbon remains in the ferrite. Therefore, improvements of both the simulation models and the validation techniques are required.

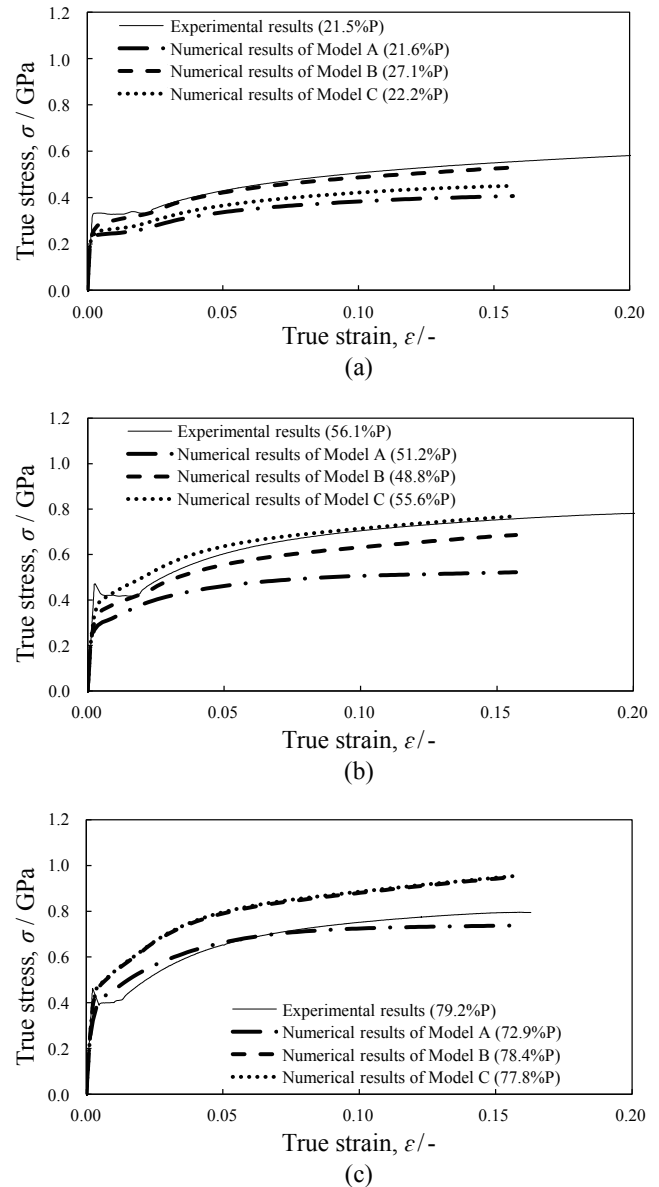


Fig. 14 Stress-strain curves of ferrite-pearlite duplex steels. The solid and the dashed lines indicate numerical and experimental results, respectively.
 (a) Pearlite volume fraction 21.5%
 (b) Pearlite volume fraction 56.1%
 (c) Pearlite volume fraction 79.2%

5. Conclusion

Our recent research was reviewed in this paper, in which a computational framework was developed to predict the macroscopic mechanical properties in multi-constituent steels. The computational approach using the finite element method enables us to obtain not only its macroscopic mechanical properties but

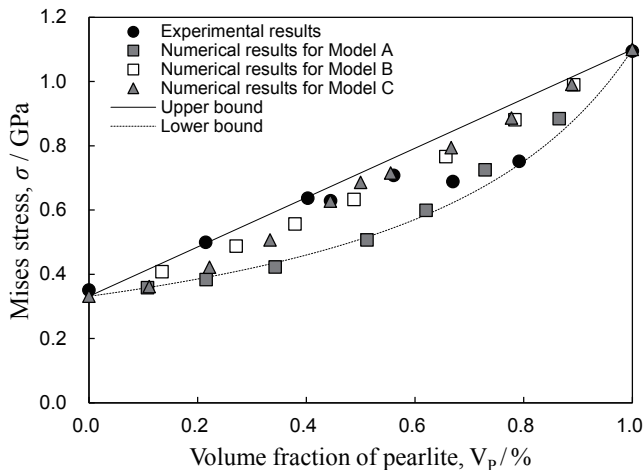


Fig. 15 Mises stresses for experimental tests and numerical simulation in identical macroscopic strain for macroscopic axial strain of 0.10.

also the material behaviors at the micro-scale as the deformation state of the microstructure, where the modeling of the microscopic heterogeneity including the anisotropy of the components is a key element; e.g., the macroscopic anisotropy caused by the heterogeneity directly relates to the formability in the plastic forming process.

Although such multiscale approaches are attractive, these remain far from practical uses, where almost all obstacles arise from the uncertainty of the micro/nanoscale material information. As partly indicated here, advanced observation techniques^(9-12,17) are applicable to validate the numerical simulations and to improve the theoretical models. In addition, atomistic simulations and advanced usage of the thermodynamic database fill in the material information difficult to obtain in experiments. We believe that such attempts lead to practical approaches.

References

- (1) *Henkei Tokusei no Yosoku to Seigyo* (ISIJ Project for the Prediction and the Control of the Deformation Characteristic) (in Japanese) (1994), The Iron and Steel Institute of Japan.
- (2) Tomota, Y., Umemoto, M., Komatsubara, N., Hiramatsu, A., Nakajima, N., Moriya, A., Watanabe, T., Nanba, S., Anan, G., Kunishige, K., Higo, Y. and Miyahara, M., "Prediction of Mechanical Properties of Multi-phase Steels Based on Stress-strain Curves", *ISIJ International*, Vol. 32, No. 3 (1992), pp. 343-349.
- (3) Weng, G. J., "The Overall Elastoplastic Stress-strain Relations of Dual-phase Metals", *J. Mech. Phys. Solids*, Vol. 38, No. 3 (1990), pp. 419-441.
- (4) Lebensohn, R. A. and Tome, C. N., "A Self-consistent Anisotropic Approach for the Simulation of Plastic Deformation and Texture Development of Polycrystals: Application to Zirconium Alloys", *Acta Metall. Mater.*, Vol. 41, No. 9 (1993), pp. 2611-2624.
- (5) Eshelby, J. D., "The Determination of the Elastic Field of an Ellipsoidal Inclusion, and Related Problems", *Proc. R. Soc. London, A*, Vol. 241, No. 1226 (1957), pp. 376-396.
- (6) Moulinec, H. and Suquet, P., "A Numerical Method for Computing the Overall Response of Nonlinear Composites with Complex Microstructure", *Comput. Methods Appl. Mech. Eng.*, Vol. 157, No. 1 (1998), pp. 69-94.
- (7) Watanabe, I., Setoyama, D., Iwata, N. and Nakanishi, K., "Characterization of Yielding Behavior of Polycrystalline Metals with Single Crystal Plasticity Based on Representative Characteristic Length", *Int. J. Plasticity*, Vol. 26, No. 4 (2010), pp. 570-585.
- (8) Watanabe, I., Setoyama, D., Nagasako, N., Iwata, N. and Nakanishi, K., "Multiscale Prediction of Mechanical Behavior of Ferrite-pearlite Steel with Numerical Material Testing", *Int. J. Numer. Methods Eng.*, Vol. 89, No. 7 (2012), pp. 829-845.
- (9) Adachi, Y., Morooka, S., Nakajima, K. and Sugimoto, Y., "Computer-aided Three-dimensional Visualization of Twisted Cementite Lamellae in Eutectoid Steel", *Acta Mater.*, Vol. 56, No. 20 (2008), pp. 5995-6002.
- (10) Wilkinson, A. J., Meaden, G. B. and Dingley, D. J., "High-resolution Elastic Strain Measurement from Electron Backscatter Diffraction Patterns: New Levels of Sensitivity", *Ultramicroscopy*, Vol. 106, No. 4 (2006), pp. 307-313.
- (11) Poulsen, H. F., "An Introduction to Three-dimensional X-ray Diffraction Microscopy", *J. Appl. Cryst.*, Vol. 45 (2012), pp. 1084-1097.
- (12) Hayashi, Y., Hirose, Y. and Setoyama, D., "In Situ Three-dimensional Orientation Mapping in Plastically-deformed Polycrystalline Iron by Three-dimensional X-ray Diffraction", *Mater. Sci. Forum*, Vol. 777 (2014), pp. 118-123.
- (13) Setoyama, D., Watanabe, I. and Iwata, N., "Comparative Study of Microscopic Morphology and Mechanical Behavior between Experiments and Numerical Analyses for Ferrite-pearlite Dual Component Steel", *Tetsu-to-Hagane* (in Japanese), Vol. 98, No. 6 (2012), pp. 290-295.
- (14) Bailey, J. E. and Hirsch, P. B., "The Dislocation Distribution, Flow Stress, and Stored Energy in Cold-worked Polycrystalline Silver", *Philos. Mag.*, Vol. 5 (1960), pp. 485-497.
- (15) Hall, E. O., "The Deformation and Ageing of Mild Steel", *Proc. Phys. Soc. B*, Vol. 64 (1951), pp. 747-753.
- (16) Petch, N. J., "The Cleavage Strength of Polycrystals", *J. Iron Steel Inst.*, Vol. 174 (1953), pp. 25-28.

(17) Sutton, M. A., Orteu, J.-J. and Schreier, H., *Image Correlation for Shape, Motion and Deformation Measurements: Basic Concepts, Theory and Applications* (2009), 321p., Springer.

Figs. 1-5

Reprinted from Int. J. Plasticity, Vol. 26, No. 4 (2010), pp. 570-585, Watanabe, I., Setoyama, D., Iwata, N. and Nakanishi, K., Characterization of Yielding Behavior of Polycrystalline Metals with Single Crystal Plasticity Based on Representative Characteristic Length, © 2010 Elsevier, with permission from Elsevier.

Figs. 6-11

Reprinted and modified from Int. J. Numer. Methods Eng., Vol. 89, No. 7 (2012), pp. 829-845, Watanabe, I., Setoyama, D., Nagasako, N., Iwata, N. and Nakanishi, K., Multiscale Prediction of Mechanical Behavior of Ferrite-pearlite Steel with Numerical Material Testing, © 2012 John Wiley & Sons, Ltd., with permission from John Wiley & Sons, Ltd.

Figs. 12, 14 and 15

Reprinted from Tetsu-to-Hagane (in Japanese), Vol. 98, No. 6 (2012), pp. 290-295, Setoyama, D., Watanabe, I. and Iwata, N., Comparative Study of Microscopic Morphology and Mechanical Behavior between Experiments and Numerical Analyses for Ferrite-pearlite Dual Component Steel, © 2012 The Iron and Steel Institute of Japan, with permission from the Iron and Steel Institute of Japan.

Fig. 13

Reprinted and partially corrected from Tetsu-to-Hagane (in Japanese), Vol. 98, No. 6 (2012), pp. 290-295, Setoyama, D., Watanabe, I. and Iwata, N., Comparative Study of Microscopic Morphology and Mechanical Behavior between Experiments and Numerical Analyses for Ferrite-pearlite Dual Component Steel, © 2012 The Iron and Steel Institute of Japan, with permission from the Iron and Steel Institute of Japan.

Noritoshi Iwata

Research Fields:

- Sheet Metal Forming
- Constitutive Modeling for Steel

Academic Degree: Dr.Eng.

Academic Society:

- The Japan Society for Technology of Plasticity

Award:

- Research Award of JSTP Tokai Chapter, 1998



Ikumu Watanabe

Research Field:

- Multiscale Modeling for Structural Materials

Academic Degree: Dr.Eng.

Academic Societies:

- The Japan Society for Computational Engineering and Science
- The Iron and Steel Institute of Japan
- The Japan Institute of Metals and Materials
- The Japan Society of Mechanical Engineer
- Japan Society for Civil Engineers
- The Minerals, Metals and Materials Society

Awards:

- JSCES Young Researcher Award, 2012
- ISIJ Young Researcher Award, 2013

Present Affiliation: National Institute for Materials Science



Daigo Setoyama

Research Fields:

- Mechanics of Materials
- Steel Engineering
- Synchrotron Diffraction

Academic Degree: Dr.Eng.

Academic Society:

- The Iron and Steel Institute of Japan

Awards:

- Best Paper Award of Atomic Energy Society of Japan, 2003
- Student Award of AESJ Kansai Office, 2004



Takamichi Iwata

Research Fields:

- Sheet Metal Forming Simulation
- Material Testing

Academic Societies:

- The Japan Society for Technology of Plasticity
- The Iron and Steel Institute of Japan

